MOLECULAR STRUCTURE, HOMO-LUMO AND VIBRATIONAL ANALYSIS OF ERGOLINE BY DENSITY FUNCTIONAL THEORY

Bhawani Datt Joshi*, **Ghanshyam Thakur**** **and Manoj Kumar Chaudhary****,*****

*Department of Physics, Siddhanath Science Campus, Tribhuvan University, Mahendranagar, Nepal.

**Department of Physics, Amrit Science Campus, Tribhuvan University, Kathmandu, Nepal.

***Central Department of Physics, Tribhuvan University, Kirtipur, Kathmandu, Nepal.

Abstract: In this work, quantum chemical study on a natural product ergoline has been presented using density functional theory (DFT) employing 6-311++G (d,p) basis set. A complete vibrational assignment has been performed for the theoretical FT-IR and Raman wavenumbers along with the potential energy distribution (PED) with the result of quantum chemical calculations. The structure–activity relationship has been interpreted by mapping electrostatic potential surface (MEP). Graphical representation of frontier molecular orbitals with their energy gap have been analyzed theoretically for both the gaseous and solvent environment employing time dependent density functional theory (TD-DFT) employing 6-31G basis set.

Keywords: Ergoline; *ab initio*; Vibrational spectroscopy; Density functional theory.

INTRODUCTION

The plant derived natural products cover a large field of medicine, which play very important role in the life threatening conditions due to their biological activity. Ergoline alkaloids (also called ergot alkaloids), the natural products occurring in the flowering plants *Rivea corymbosa* and *Ipomoea violacea* (Convolvulaceae; called morning glory) and taxonomically unrelated fungal, are known to inhibit the release of prolactin[1,2]. Ergot alkaloids, the derivatives of the tetracyclic ergoline scaffold, divided into three main groups; display a diverse spectrum of pharmacological properties; including central, peripheral, and neurohormonal activities that arise from their activities at various monaminergic receptors[3]. Naturally occurring alkaloids like; the D-lysergic acid amides, produced by the "ergot fungus" *Claviceps purpurea*, have been used as medicinal agents for a long time. They are active ingredients in medications designed to treat migraine disease or are used in childbirth and weaning[4-6].

Ergoline alkaloids are also used as hallucinogens by native Central American people in religious ceremonial practices[7]. Historically, some ergots (e.g., ergoline and ergopeptine) have been used as probes to study various 5-HT receptor subtypes[8-12]. However, during the middle Ages, they were known for poisoning and sever toxicosis in cattle feeding with ergoline alkaloid producing clavicipitaceous fungi[13-16].

Alkaloids occupy unique place in the natural product.

Their complex structures and dynamical behaviors attract the chemists towards the challenging problems in structural elucidation and synthesis. Vibrational spectroscopy is a valuable method for determining dynamical behavior and the electronic structure of the alkaloids microscopically[17]. Raman and infrared (IR) are the traditional methods of vibrational analysis for the structural characterization of the substances[18]. They have been widely used to study energetic, thermal, electronic and dynamical behavior from vibrational dynamics of the

***Author for Correspondence*:** Bhawani Datt Joshi**,** Department of Physics, Siddhanath Science Campus, Tribhuvan University, Mahendranagar.
E-mail: pbdjoshi@gmail.com, bdjoshi_007@yahoo.com

Received: 30 April 2019; First Review: 20 Aug 2020; Second Review: 25 Aug 2020; Accepted: 28 Aug 2020.

Doi: https://doi.org/10.3126/sw.v14i14.34978

large number of biomolecules. In the recent years, the application of *ab initio* methods has also become a part of keen interest as they provide additional vibrational spectroscopic data[17,19.20]. In this study, the theoretical vibrational spectra of ergoline (6aR)-4,6,6a,7,8,9,10a-Octahydroindolo[4,3-*fg*] quinoline) with the identification of various normal modes have been investigated. The aim of this study was to study the molecular structure, vibratonal wavenumbers and the electronic absorption band theoretically. The molecular structure, harmonic vibrational wavenumbers, electrostatic potential surfaces, absolute Raman scattering activities and IR absorption intensities have been calculated by density functional theory (DFT)[21] using Gaussian 09 program package[22] employing B3LYP/6-311++G(d,p) basis set[23,24]. The highest occupied molecular orbital (HOMO), lowest unoccupied molecular orbital (LUMO), energy band gap (ΔE) and the dipole moment were determined for the optimized structure. A theoretical time dependent density functional theory (TD-DFT) [25,26] method has been used to calculate absorption parameters in gas phase employing 6-31G basis set. Graphical representation of HOMO and LUMO can provide valuable information that elucidates the nature of reactivity and some of the structural and physical properties of the molecule.

METHODOLOGY

Computational methods

The electronic structure and the optimized geometry of the molecule were computed by *ab initio* Hartree-Fock (HF) and the density functional functional theory (DFT) method using Gaussian 09 program[22] employing 6-311++G(d,p) basis set. The DFT calculations were carried out in the frame-work of Becke-Lee-Yang-Parr [B3LYP] functional, in which the exchange functional is local spin density exchange with Becke gradient correlation[27] and the correlation functional is that of Lee, Yang and Parr with both local and non local terms[28,29]. The molecular structure, vibrational frequencies and energy of optimized geometric structure of the molecule were calculated at B3LYP/6-311++G (d,p) level using Gaussian 09 program[22].

The absolute Raman scattering and IR absorption intensities are calculated in the harmonic approximation in the same level. The optimized ground state structure of ergoline is shown in figure 1. The normal mode analysis was performed and the potential energy distribution (PED) was calculated using localized symmetry using GAR2PED[30]. For this purpose a complete set of 90 internal co-ordinates was defined by Pullay's recommendation[31,32] . The graphical representation of MEP mapping and, the calculated IR and Raman spectra were made using Gauss View program[33]. Visualization and confirmation of calculated data were done by using the CHEMCRAFT program[34]. The frontier energy orbitals HOMO (characterized by highest occupied molecular orbital) and LUMO (characterized by lowest unoccupied molecular orbital), and band gap (ΔE) were calculated using TD-DFT[25,26] employing 6-31G basis for both the gaseous and solvent phase.

RESULTS AND DISCUSSION

Geometry optimization

Using the standard geometric parameters[35], geometry optimization was performed as the first task in *ab initio* calculation without using any constraints. The optimized geometric parameters were used in the vibrational frequency calculations to characterize all the stationary points as minima. The related energies of the molecule are calculated employing *ab initio* HF functions and DFT functional. The energy calculated by DFT (- 652.8040 Hartree) is lower showing more stable than that by HF (-648.5243 Hartree) due to some electron correlations in the former. The enthalpy difference between these two theories is 12.0725 kcal/mol. The optimized ground state structure (in the gas phase) is as shown in figure 1.

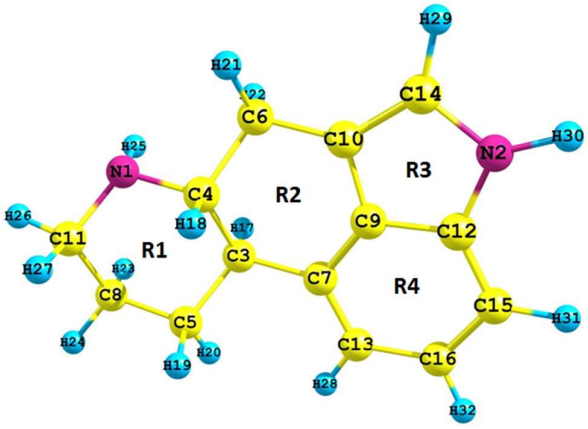

Figure 1: Optimized structure of ergoline.

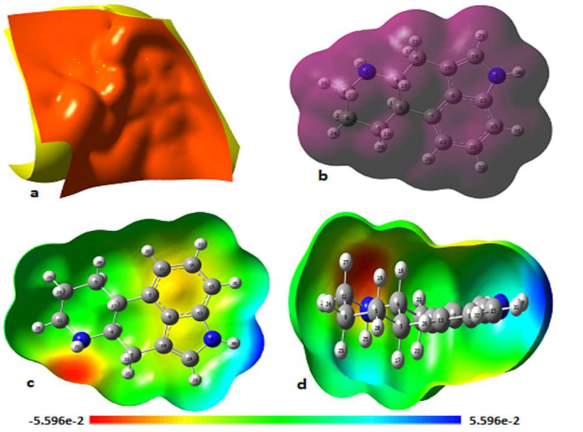

Figure 2: Graphical plots of: (a) electrostatic potential surface (b) electron density (c) molecular electrostatic potential mapped in-plane and (d) molecular electrostatic potential mapped perpendicular to the plane (from -5.596e-2 esu to +5.596e-2 esu).

Molecular electrostatic potential

The molecular electrostatic potential (MEP) in a molecule at a point r(x,y,z) is the force on unitary positive test charge at that point due to its whole electrical charge and is given by:

$$V(r) = \sum_{A=1}^{N} \frac{Z_A}{|\vec{R}_A - \vec{r}|} - \int \frac{\rho(\vec{r'})dr}{|\vec{r'} - \vec{r}|}$$

where Z_A is the charge on nucleus A located at R_A and $\rho(r')$ is the electron density. The first term is due to the nucleus and the second due to electron cloud.

The MEP provides a visual method to understand the relative polarization of molecule[17]. Such surfaces depict the size, shape, charge density, and site of chemical reactivity of the molecules. In the surface generated, negative electrostatic potential (shades of red color) corresponds to an attraction of the proton by the concentrated electron density in the molecules (from lone pairs, pi-bonds, etc.) and positive electrostatic potential (shades of blue color) corresponds to repulsion of the proton by the atomic nuclei in the regions where low electron density exists and the nuclear charge is incompletely shielded. The largely white or lighter color shades on the surface indicate that the molecule is mostly non-polar. The potential increases in the order red < orange < yellow <green<blue.

The molecular electrostatic potential (MEP), electron density (ED) and the electrostatic potential surface ESP) mapped with the output obtained by B3LYP/6-311++G (d,p) basis are shown in figures 2(a-d). From the figure, the highest negative potential (red region) is localized over the nitrogen atom N1. A less negative area occurs over the ring R2 and R3. The lowest potential with the blue region is localized over the hydrogen atom connected with N2 atom. The ED plot shows uniform charge distribution over the molecular surface.

UV-visible spectroscopy

UV-vis spectroscopy provides some valuable information about the nature of electronic transitions between the two prominent frontier molecular orbitals named as; HOMO (characterized by highest occupied molecular orbital) and LUMO (characterized by lowest unoccupied molecular orbital). The nature of electronic transition has been studied by using TD-DFT employing 6-31G basis set[25,26] for both the gas and solvent (MeOH) phases. The theoretical absorption spectra are shown in the figure 3. The calculated electronic transitions with high oscillator strength are listed in Table 1.

Table 1. Electronic transitions with absorption wavelength (λ_{max} in nm), excitation energy (eV), oscillator strength, frontier orbital energies (eV) and the dipole moment (μ in D).

Excited states	Gas Phase				MeOH Phase				Transition type
	Transitions	eV	λ_{max}	Oscillator strength	Transitions	eV	λ_{max}	Oscillator strength	
1	H → L	4.7240	262.45	0.1017	H → L	4.6077	269.08	0.1338	$\pi \rightarrow \pi^*$
2	H -3 → L	6.1719	200.89	0.2617	H → L +1	5.8791	210.89	0.3184	„
3	H → L+2	6.3689	194.67	0.1881	H-1→ L+1	6.0278	205.69	0.1682	„
4	H-1→ L+2	6.5217	190.11	0.0798	H-3 → L	0.1682	198.09	0.1968	„
5	H-2→ L+1	6.7531	183.60	0.2367	H-2 →L+1	6.5887	188.18	0.3575	..
6	H-2→ L+2	7.0700	175.37	0.1412	H-2 →L+2	6.9796	177.64	0.1235	„
7	H -3→L+1	7.5295	164.66	0.1117	H-3 →L+1	7.4289	166.89	0.1739	„
8	H -3→L+2	8.4539	146.66	0.1868	H-3 →L+2	8.3861	147.85	0.1552	„

	E_{HOMO}	E_{LUMO}	ΔE	μ (D)
Gas	- 5.147798	0.035511	5.183310	1.3941
MetOH	- 5.277569	- 0.162751	5.114818	1.8221

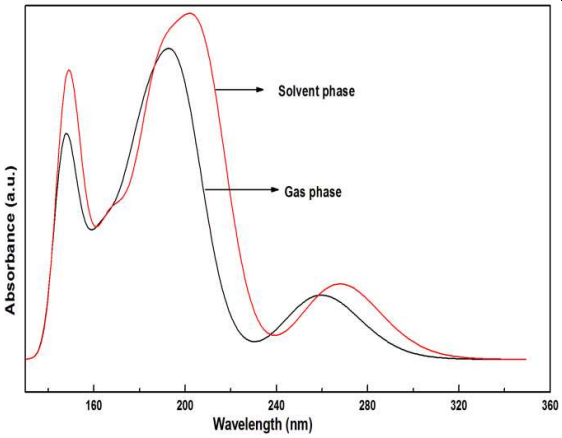

Figure 3: Plot of theoretical UV-vis spectra taken in gas (black) and the solvent (red).

HOMO and LUMO, the frontier molecular orbitals (FMOs), are very important quantum chemical parameters. These two vicinal orbitals play the same role of electron donor and acceptor, respectively. Their energy gap is an important stability index. A higher value of the energy difference more is the stability of the molecular system[36]. The HOMO-LUMO plots are given in figure 4. TD-DFT calculations predict the intense electronic transitions at 262.45 nm (H → L), 200.89 nm (H-3 → L), 183.60 nm (H-2 → L+1) and 146.66 nm (H-3 → L+2) with oscillator strengths 0.1017, 0.2617, 0.2367 and 0.1868, respectively in the gaseous phase. Similarly, in the solvent phase, the transitions are centered at 269.08 nm (H → L), 205.69 nm (H-1 → L+1), 210.89 nm (H → L+1), 188.18 nm (H-2 → L+1) and 147.85 nm (H-3 → L+2) with the oscillator strengths 0.1338, 0.1682, 0.3184, 0.3575 and 0.1552, respectively. On the basis of calculated molecular orbital coefficient analysis, the main electronic excitations are due to $\rightarrow \pi^*$ transitions.

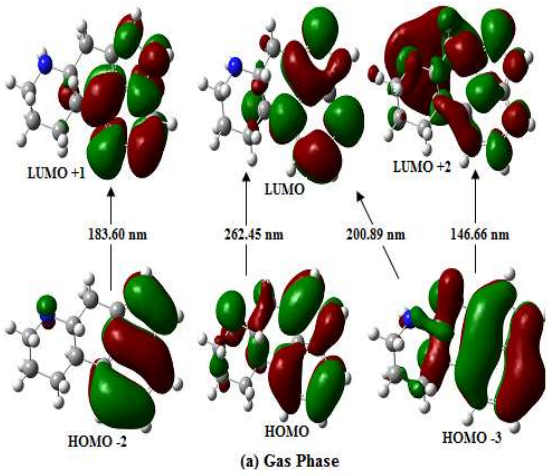

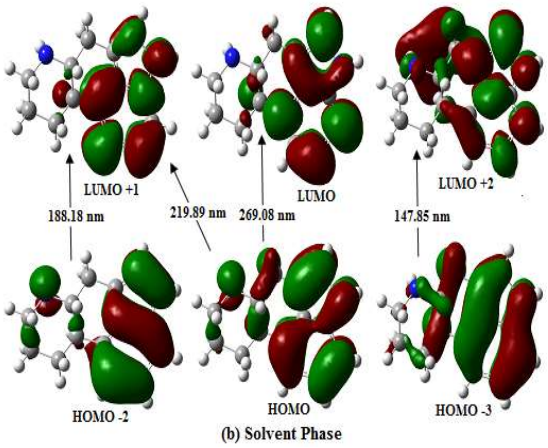

Figure 4: HOMO-LUMO plots (a) Gas phase and (b) Solvent phase.

Vibrational analysis

This molecule has 32 atoms and hence gives 90 (3N-6; N number of atoms) modes of vibration. All the modes are both Raman and IR active. Some selected fundamental vibrational wavenumbers, intensities and the PED distribution obtained by HF and DFT methods with 6-311++G (d,p) basis set are given in Table 2. Details of vibrational wavenumbers and their PED is listed in Table S (supplementary Material). The wavenumbers obtained by DFT have smaller values than that by HF methods due to inclusion of electron correlations in it. The assignments are given as per the internal coordinate system recommended by Pulay *et al*. 1979[31] using DFT. The theoretical wavenumbers, generally higher than the observed values, were corrected by a scaling factor given by Yoshida *et al*.[37] using the expression: υ_{obs} = (1.0087 – 0.0000163 υ_{cal}) υ_{cal}. The Raman scattering cross-sections, $\partial\upsilon_j/\partial\upsilon$, which are proportional to the Raman intensities may be calculated from the Raman scattering amplitude and predicted wavenumbers for each normal modes using the relationship[38,39]:

$$\frac{\partial\sigma_j}{\partial\Omega} = \left(\frac{2^4\pi^4}{45}\right)\left(\frac{(\upsilon_0-\upsilon_j)^4}{1-exp\ \frac{-hc\upsilon_j}{kT}}\right)\left(\frac{h}{8\pi^2 c\upsilon_j}\right)S_j$$

where S_j and υ_j are the scattering activities and the predicted wavenumbers (in cm^{-1}), respectively of the j^{th} normal mode, υ_o is the Raman exciting wavenumber (in cm^{-1}), and h, c and k are universal constants. The FT-IR and Raman spectra are given in figures 5 and 6, respectively. The assignments of some prominent modes are discussed below:

Ring R1 vibrations

The N–H stretching absorption generally occurred in the region 3500–3220 cm^{-1} [40]. In this study, pure N-H stretching vibration was calculated at 3320 cm^{-1} with IR intensity 0.4759 and Raman activity 73.268 units, respectively. The mixed in-plane-bending was calculated at 1473 cm^{-1}.

The CH_2 asymmetric stretching vibration was calculated at 2937, 2930 and 2919 cm^{-1}. The symmetric stretching of the mode was predicted at 2889, 2886 and 2878 cm^{-1}. The wagging vibration was predicted at 1371, 1366 and 1351 cm^{-1} in the scaled DFT. The twisting vibrations were calculated at 1308, 1274 and 1194 cm^{-1}. The C4-H /C3-H stretching vibrations calculated at 2877/2833 cm^{-1} have intensities 42.173/11.63 units in the IR spectra and 115.142/106.889 units in the Raman spectra. The highly mixed rocking vibrations related to these modes were calculated at 1345 and 1338 cm^{-1}.

Table 2. Selected calculated IR and Raman wave numbers (cm^{-1}) of ergoline.

DFT		HF	Raman activity (Å^4/a.m.u.)	IR intens. (km-mol^{-1})	Potentian energy distribution (PED%)
Unscaled	Scaled	scaled			
3676	3488	3703	176.582	80.067	R3[υ(NH)](100)
3488	3320	3540	73.268	0.4759	R1[υ(NH)]100)
3241	3098	3233	134.288	1.289	R3[υ(CH)](98)
3185	3047	3194	269.652	23.062	R4[υ(CH)](100)
3174	3037	3183	83.815	19.732	R4[υ(CH)](97)

3161	3026	3165	63.869	1.458	R4[υ(CH)](86)
3069	2942	3082	112.236	23.105	R2[$\upsilon_a(CH_2)$](96)
3063	2937	3069	156.889	56.344	R1[$\upsilon_a(CH_2)$](97)
3056	2930	3064	50.957	37.593	R1[$\upsilon_a(CH_2)$](96)
3044	2919	3050	231.545	81.004	R1[$\upsilon_a(CH_2)$](96)
3010	2889	3025	71.513	51.843	R1[$\upsilon_s(CH_2)$(86)+υ(C4H)(8)]
3007	2886	3020	33.024	27.533	R1[$\upsilon_s(CH_2)$](93)
2999	2878	3015	127.905	14.386	R1[$\upsilon_s(CH_2)$(60)+υ(C4H)(27)]
2997	2877	3005	115.142	42.173	R1[υ(C4H)(45)+$\upsilon_s(CH_2)$(43)]
2978	2859	3002	144.925	18.564	R2[$\upsilon_s(CH_2)$](71)+R1[υ(C4H)](15)
2949	2833	2976	106.889	11.763	R1[υ(C3H)](90)
1651	1621	1764	27.684	6.155	R4[(CC)(45)+δ_{trig}(26)]+R2[δ_{trig}](15)+R3[υ(C=C)](12)
1633	1604	2976	27.304	12.490	R3[δ'_{ring}(33)+υ(CC)(12)]+R2[υ(CC)](33)+R4[δ_a](14
1590	1563	1701	72.071	8.583	R3[υ(C=C)(48)+δ'_{ring}(18)+]+R4[δ'_a](14)+R2[δ_{trig}](6)
1535	1510	1632	3.843	3.897	R4[δ_{in}(CH)](48)+R3[δ_{in}(NH)](23)+R2[υ(CC)](19)
1499	1475	1608	1.483	3.198	R1[$\delta(CH_2)$(68)+$\rho(CH_2)$(19)]
1496	1473	1597	0.777	13.512	R1[δ_{in}(NH)(46)+ρ(C4H)(23)+$\delta(CH_2)$(19)]
1487	1464	1585	14.838	3.032	R1[$\delta(CH_2)$(27)+δ_{trig}(14)+R2[$\delta(CH_2)$(22)+δ'_{ring}(15)]
1485	1462	1581	6.954	5.071	R2[$\delta(CH_2)$](46)+R1[$\delta(CH_2)$](34)
1479	1456	1577	12.824	17.448	R1[$\delta(CH_2)$(37)+ δ_{in}(NH)(30)+$\rho(CH_2)$(11)]
1458	1436	1551	11.749	21.852	R4[δ'_a(30)+δ_{in}(CH)(21)]+R3[υ(CC)](26)+R2[δ_{trig}](11)
1444	1423	1538	60.106	10.565	R3[δ_{in}(NH)(25)+υ(NC)(17)+R2[υ(CC)](30)+R4[δ'_a](15)
1395	1375	1499	39.051	2.082	R3[δ'_{ring}(21)+υ(CC)(14)]+R2[υ(CC)](27)+R4[δ_{trig}(15)
1390	1371	1494	16.434	1.897	R1[ω(18) γ(8)(CH_2)+ρ(CH)(15)]+R2[ω(CH_2)(18)+υ(CC)(11)]
1385	1366	1479	0.763	1.014	R1[ω(CH_2)(42)+δ_{trig}(23)]+R2[ρ(C3H)(12)+δ'_a(9)]
1373	1354	1475	4.532	6.295	R1[ω(CH_2)(35)+δ_{trig}(14)]+R4[υ(CC)](21)
1372	1353	1472	1.715	18.654	R2[ω(CH_2)(24)+υ(CC)(8)]+R1[ω(CH_2)](31)+R3[υ(CC)](18)
1356	1338	1426	7.158	9.850	R1[ρ'(CH)(39)+γ(CH_2)(15)]+R2[γ(CH_2)(17)+δ'_a(15)]
1309	1292	1377	18.185	15.722	R2[υ(CC)(35)+δ'_a(5)]+R4[δ_{in}(CH)(14)+δ_{trig}(12)]+R3[υ(NC)](23)
1290	1274	1369	5.039	1.007	R1[γ(CH_2)](46)+ R2[δ'_a(20)+R2[γ(CH_2)](20)
1285	1269	1367	4.722	1.603	R4[δ_{trig}(44)+υ(CC)(5)]+R3[δ'_{ring}(20)+υ(CC)(9)]
1253	1238	1332	2.294	17.712	R2[δ'_a(40)+δ_{trig}(7)]+R4[δ_{trig}](28)+R3[δ'_{ring}](10)
1240	1226	1324	9.112	7.109	R1[δ_{trig}](44)+R2[δ_{trig}](22)+R3[υ(NC)(9)+υ(CC)(5)]
1234	1220	1313	14.237	3.165	R4[δ_{trig}](44)+R3[υ(CC)(13)+δ'_{ring}(12)+υ(NC)(12)]+R2[δ'_a](8)

1207	1194	1288	0.981	0.981	R2[$\gamma(CH_2)$](53)+R1[$\gamma(CH_2)$](11)+R3[υ(NC)](8)
1183	1170	1261	4.232	2.784	R4[δ_{in}(CH)(21)+υ(CC)(14)+δ_{trig}(13)]+R2[υ(CC)](13)
1178	1166	1238	2.871	0.0854	R2[δ_{trig}(50)+δ'_a(12)]+R1[δ_{trig}](15)+R3[δ'_{ring}](6)
1147	1136	1223	5.845	33.362	R2[puck](48)+ R2[υ(CC)](7)+R1[δ'_a](25)
1132	1121	1211	6.585	14.422	R1[δ_{trig}](44)+R2[δ_{trig}(17)+δ'_a(15)+R4[δ'_{ring}](8)
1116	1105	1100	1.220	13.348	R4[δ_{trig}](45)+R3[δ'_{ring}](27)+R2[δ_{trig}](13)
1101	1091	1174	3.647	7.290	R2[δ_{trig}(42)+δ'_a(17)]+R3[υ(NC)](15)+R1[υ(CC)](8)
1088	1078	1148	1.298	22.097	R3[δ'_{ring}(37)+υ(NC)(33)]+R2[δ'a](10)
1069	1060	1139	2.787	3.401	R4[δ_{trig}](39)+R2[υ(CC)](21)+R3[δ'_{ring}](11)
920	914	986	6.390	4.841	R4[δ_{trig}(57)+δ_a(8)]+R2[δ_{trig}](12)+R3[δ'_{ring}](12)
897	892	978	1.551	8.033	R2[puck(48)+δ'_a(11)]+R3[δ'_{ring}](18)+R4[puck](7)
881	876	958	0.728	3.817	R2[δ_{trig}(37)+δ'_a(15)]+R4[oop(CH)](27)
862	857	919	6.980	1.149	R4[puck(56)+δ'_a(24)]
849	845	916	1.246	1.093	R4[δ_{trig}(41)+δ'_a(37)]+R3[δ'_{ring}](15)
821	817	903	2.313	32.478	R2[δ'_a(42)+ υ(CC)(6)]+R1[υ(CC)](38)
730	728	788	3.384	42.321	R4[δ_a(20)+δ_{trig}(15)]+ R3[δ_{ring}](26)+R2[δ'_a](25)
635	634	684	2.487	7.073	R2[δ_{trig}](39)+R3[δ'_{ring}](35)+R4[δ_a](19)
615	614	665	3.672	1.377	R3[δ'_{ring}](69)+R4[δ_a](12)+R2[δ_{trig}](9)
602	601	649	8.028	0.419	R4[δ'_a](58)+R2[δ_{trig}(19)+δ'_a(8)+R3[δ'_{ring}](5)
595	594	637	2.146	1.526	R3[δ'_{ring}](46)+R4[δ'_a](43)
551	551	589	6.959	1.725	R4[δ'_a](51)+R2[δ'_a(36)+δ_{trig}(5)]

Proposed assignments and potential energy distribution (PED) for vibrational normal modes.

Types of vibration: ν, stretching; δ, deformation (bending), scissoring; oop, out-of-plane bending; ω, wagging; γ, twisting; ρ, rocking; τ, torsion.

Potential energy distribution (contribution ≥ 5).

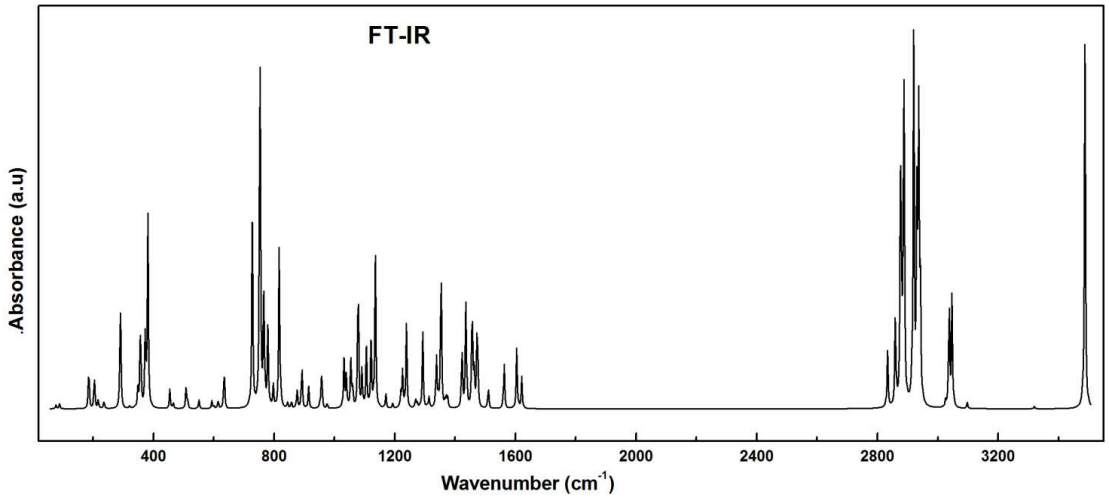

Figure 5: Calculated FT-IR spectrum between the ranges 200-3500 cm^{-1}.

Ring R2 vibrations

The asymmetric stretching of CH_2 predicted at 2942 cm^{-1} has intensity 23.105/112.236 units in the IR/Raman spectra. The symmetric stretching was calculated at 2859 cm^{-1}. The deformation, wagging and twisting mode vibrations were calculated at 1462, 1353 and 1194 cm^{-1}, respectively.

Highly mixed C-C ring stretching was predicted at 1292 cm^{-1}. The ring deformation and puckering vibrations are below 1200 cm^{-1} in the mixed modes.

Ring R3 vibrations

The N-H stretching vibration was calculated at 348 cm^{-1}. This pure mode (100% contribution in PED) has intensity 176.582 units in the Raman spectra and 80.067 units in the IR spectrum. The in-plane vibration of this mode was predicted at 1423 cm^{-1}, while out-of-plane vibration was at 381cm^{-1} as listed in the Table 2.

The frequency of ring deformation vibration was calculated at 1604 cm^{-1}. The C=C stretching predicted at 1563 cm^{-1} is a mixed mode. The mixed NC stretching is below 1430 cm^{-1}.

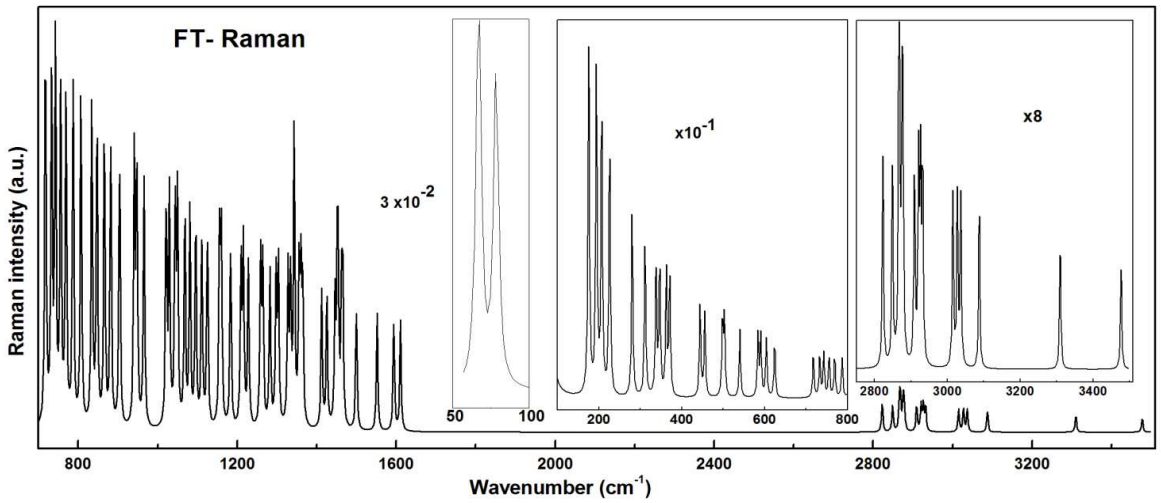

Figure 6: Calculated FT-Raman spectrum between the ranges 50-3500 cm^{-1} (intensity magnitudes shown in the insets are modified as: 50-100 cm^{-1} by $3x10^{-2}$, 100-800 cm^{-1} by 10^{-1} and 2750-3500 cm^{-1} by 8 times, respectively).

Ring R4 vibrations

One can easily expect three modes of stretching vibration related to each CH moiety. In this study, the C-H stretching vibration was predicted at 3047, 3037 and 3026 cm^{-1}. The in-plane deformation was calculated at 1510 cm^{-1}. The out-of-plane vibration of this mode is 951 cm^{-1}. In the ring, C-C stretching and deformation vibrations were predicted at 1621 and 1436 cm^{-1}, respectively. The trigonal ring deformations were calculated below 1269 cm^{-1}.

CONCLUSION

The investigated molecule has 90 modes of vibrations. All the modes are both IR and Raman active. In this study, the vibrational wavenumbers along with their potential energy distribution has been analyzed by *ab initio* and DFT methods. Information about the shape, size, charge density and the structure-activity relation have been analyzed by mapping MEP. The large value of the band gap obtained from the HOMO and LUMO analysis supports that the title molecule is stable; however, there occur intra-molecular charge transfer (ICT) within the molecule. This study could be a better starting for further investigations on structure-activity relation of the compound.

ACKNOWLEDGEMENTS

B.D. Joshi would like to acknowledge Professor Poonam Tandon, HoD, Physics Department, Lucknow University, India for providing software facilities.

REFERENCES

1. Rusterholz, D.B., Barfknecht C. F. & Clemens, J. A. 1977. *Ergoline congeners as potential* inhibitors of prolactin release. 3. Derivatives of 3-phenylpiperidine. *Journal of Medicinal Chemistry.* **20 (1):** 85–88. http://dx.doi.org/10.1021/jm00211a017
2. Ahimsa-Müller, M.A., Markert, A., Hellwig, S., Knoop, V., Steiner, U., Drewke C. & Leistner, E. 2007. Clavicipitaceous fungi associated with ergoline alkaloid-containing Convolvulaceae. *Journal of Natural Products*. **70(12):** 1955-1960. http://dx.doi.org/10.1021/np070315t
3. Krogsgaard-Larsen, N., Jensen, A.A., Schrøder, T.J., Christoffersen, C.T. & Kehler, J. 2014. . Novel Aza-analogous Ergoline Derived Scaffolds as Potent Serotonin 5-HT_6 and Dopamine D_2 Receptor Ligands. *Journal of Medicinal Chemistry.* **57(13):** 5823-5828**. http:**//dx.doi.org/10.1021/jm5003759
4. Gröcer D. & Floss, H.G. 1998. G.A. Cordell (Editors). *The alkaloids: Chemistry and Biology.* Biochemistry of ergot alkaloids-achievements and challenges. Academic Press, San Diego, **50**: 171.
5. Schardl, C.F., Pannacione, D.G. & Tudzynski, P. 2006. G. A. Cordell (Ed). *The Alkaloids: Chemistry and Biology.* Ergot alkaloids-biology and molecular biology. Academic Press, New York, **63:** p 45.
6. Markert, A. *et al*., 2008. Biosynthesis and Accumulation of Ergoline Alkaloids in a Mutualistic Association between *Ipomoea asarifolia* (Convolvulaceae) and a Clavicipitalean Fungus. *Plant Physiology*. **147(1):** 296-305. http://dx.doi.org/10.1104/pp.108.116699 Hofmann, A. 1961. Die Wirkstoffe der Mexikanischen Zauberdroge "Ololiuqui"[1]. *Planta Medica*. **9(4):** 354-367. http://dx.doi.org/10.1055/s-0028-1100366
7. Clay, K. 1991. In P. Barbosa, V. A. Krischik, C.G. Jones (Eds). Microbial Mediation of Plant-HerbiVore Interactions. John Wiley & Sons, New York, p. 199.
8. Gröger, D. 1972. In S. Ajl (Ed.). *Microbial Toxin*. Academic Press, New York. **8:** 321.
9. Rosse, G. & Schaffhauser, H. 2010. 5-HT6 receptor antagonists as potential therapeutics for cognitive impairmrnt. *Current Topics in Medicinal Chemistry*. **10(2):** 207-221. http://dx.doi.org/10.2174/156802610790411036
10. Medeiros, R.M.T., Barbosa, R.C., Riet-Corea, F., Lima, E.F., Tabosa, I.M., de Barros, S.S., Gardner D.R. & Molyneux, R.J. 2003. Tremorgenic syndrome in goats caused by Ipomoea asarifolia in Northeastern Brazil. *Toxicon*. **41(7):** 933-335. http://dx.doi.org/10.1016/S0041-0101(03)00044-8
11. Choudhary, M.S., Sachs, N., Uluer, A., Glennon, R. A., Westkaemper, R. B. & Roth, B. L. 1995. Differential ergoline and ergopeptine binding to 5-hydroxytryptamine2A receptors: ergolines require an aromatic residue at position 340 for high affinity binding. *Molecular Pharmacology*. **47:** 450-457. http://dx.doi.org/0026-895x/95/0300450
12. Ramírez, M. J. 2013. 5-HT 6 receptors and Alzheimer's disease. *Alzheimer's research & therapy*. **5(2):** 1-8. http://dx.doi.org/10.1186/alzrt169
13. Geldenhuys, W.J. & Van der Schyf, C.J. 2008. Serotonin 5-HT6 Receptor Antagonists for the Treatment of Alzheimers Disease. *Current Topics in Medicinal Chemistry*. **8(12):** 1035-1048. http://dx.doi.org /10.2174/156802608785161420
14. Novi, F., Millan, M.J., Corsini, G.U. & Maggio, R. 2007. Partial agonist actions of aripiprazole and the candidate antipsychotics S33592, bifeprunox, *N*-desmethylclozapine and preclamol at dopamine D_{2L} receptors are modified by co-transfection of D_3 receptors: potential role of heterodimer formation. *Journal of Neurochemistry*. **102(4):** 1410-1424. http://dx.doi.org/10.1111/j.1471-4159.2007.04660.x
15. Wang, C., *et al*., 2013. Structural Basis for Molecular Recognition at Serotonin Receptors. *Science*. **340(6132):** 610-614. http://dx.doi.org /10.1126/science.1232807
16. Mishra, R., Joshi, B.D., Srivastava, A., Tandon P. & Jain, S. 2014. Quantum chemical and experimental studies on the structure and vibrational spectra of an alkaloid–Corlumine. *Spectrochimica Acta Part A: Molecular and Biomolecular Spectroscopy.* **118:** 470 - 480. http://dx.doi.org/10.1016/j.saa.2013.09.015
17. Chamers, J.M. & Griffiths, P.R. (Eds.), 2002. Handbook of Vibrational Spectroscopy, John Wiley and Sons. ISBN-13: 978-0471988472
18. Joshi, B.D., Mishra, R., Tandon, P., Oliveira, A.C. & Ayala, A.P. 2014. Quantum chemical studies of structural, vibrational, NBO and hyperpolarizability of ondansetron hydrochloride. *Journal of Molecular Structure*. **1058:** 31-40. http://dx.doi.org/10.1016/j.molstruc.2013.10.062
19. Joshi, B.D. Tandon P. & Jain, S. 2013. Structure, MESP and HOMO-LUMO study of 10-Acetyl10H-phenothiazine 5-oxide using vibrational spectroscopy and quantum chemical methods. *BIBECHANA*. **9:** 38-49. BMHSS, p.38-49.
20. Hohenberg, P. Kohn, W. 1964. Inhomogeneous Electron Gas. *Physical Review B*-**136(3):** 864-871. http://dx.doi.org/10.1103/PhysRev.136.B864
21. Frisch, M.J. *et al*., 2009. GAUSSIAN 09, Revision, Gaussian Inc, Wallingford, CT.
22. Becke, A.D. 1993. Density-functional thermochemistry. III. The role of exact exchange. *Journal of Chemical Physics*. **98:** 5648-5652. http://dx.doi.org/10.1063/1.464913
23. Parr, R.G. & Yang, W. Density Functional Theory of Atoms and Molecules, Oxford University Press, Oxford, New York, p 333.
24. Petersson, G.A. &. Allaham, M.A. 1991. A complete basis set model chemistry. II. Open-shell systems and the total energies of the first-row atoms. *Journal of Chemical Physics.* **94(9):** 6081-6090. http://dx.doi.org/10.1063/1.460447
25. Glendering, E.D., Reed, A.E., Carpenter, J. E. & Weinhold, F. 1998. NBO Version 3.1, TCI, University of Wisconsin, Madison.
26. Casida, M.E. 1995. D. P Chong (Eds.). Developments in Density Functional Theory. *World Scientific, Singapore*. **1:** 155.

27. Casida, M. E. Casida K. C. and Salahub, D. R. 1998. Excited-state potential energy curves from time-dependent density-functional theory: A cross section of formaldehyde's $^1A_1$ manifold. *International journal of Quantum Chemistry*. **70:** 933-941. http://dx.doi.org/ OI: 10.1002/(SICI)1097-461X
28. Lee, C. Yang W. &. Parr, R.G. 1998. Development of the Colle-Salvetti correlation-energy formula into a functional of the electron density. *Physical Review.* B-**37:** 785-789. http://dx.doi.org/ 10.1103/PhysRevB.37.785
29. Martin, J.M.L. & Van Aslenoy, C. 1995.Gar2ped, University of Antwerp.
30. Pulay, P., Fogarasi, G., Pang, F. & Boggs, J.E. 1979. Systematic *ab initio* gradient calculation of molecular geometries, force constants, and dipole moment derivatives, *Journal of American Chemical Society*. **101:** 2550 2560. http://dx.doi.org/10.1021/ja00504a009
31. Pulay, P., Fogarasi, G., Pongor, G., Boggs, J.E. & Vargha, A. 1983. Combination of theoretical *ab initio* and experimental information to obtain reliable harmonic force constants. Scaled quantum mechanical (QM) force fields for glyoxal, acrolein, butadiene, formaldehyde, and ethylene. *Journal of American Chemical Society*. **105(24):** 7037-7047. http://dx.doi.org/10.1021/ja00362a005
32. Frisch, A., Nielson, A.B. & Holder, A.J. 2000. GaussView User Manual, Gaussian Inc, Pittsburgh, P.A.
33. Zhurko, G.A. & Zhurko, D.A. 2005. Chemcraft . <http:// www. chemcraftprog.com>.
34. https://pubchem.ncbi.nlm.nih.gov/search/search.
35. Singh, R.N., Kumar, A., Tiwari, R.K., Rawat, P., Baboo, V. & Verma, D. 2012. Molecular structure, heteronuclear resonance assisted hydrogen bond analysis, chemical reactivity and first hyperpolarizability of a novel ethyl-4-{[(2,4-dinitrophenyl)-hydrazono]-ethyl}-3,5-dimethyl-1*H*-pyrrole-2-carboxylate: A combined DFT and AIM approach. *Spectrochimica Acta Part A: Molecular and Biomolecular Spectroscopy*. **92:** 295-304. http://dx.doi.org /10.1016/j.saa.2012.02.086
36. Yoshida, H. Takeda, K., Okamura, J., Ehara, A. & Matsurra, H. 2002. A New Approach to Vibrational Analysis of Large Molecules by Density Functional Theory: Wavenumber-Linear Scaling Method. *Journal of Physical Chemistry. A*-**106(14):** 3580-3586. http://dx.doi.org/10.1021/jp013084m
37. Guirgis, G.A., Klaboe, P., Shen, S., Powell, D.L., Gruodis, A., Aleksa, V., Nielsen, C.J. Tao, J., Zheng, C. & Durig, J.R. 2003. Spectra and structure of silicon-containing compounds. XXXVI† — Raman and infrared spectra, conformational stability, *ab initio* calculations and vibrational assignment of ethyldibromosilane. *Journal of Raman Spectroscopy.* **34(4):** 322-336. http://dx.doi. org/10.1002/jrs.989
38. Polavarapu, P. L. 1990. *Ab initio* vibrational Raman and Raman optical activity spectra. *Journal of Physical Chemistry*. **94(21):** 8106-8112. http://dx.doi.org/10.1021/j100384a024
39. Silverstein, R.M. Bassler G.C. & Morrill, T.C. 1991. *Spectrometric Identification of Organic Compounds (Fifth Edition)*. Wiley, New York. p 430. ISBN 0471 63404 2.